IEEE Access
Multidisciplinary | Rapid Review | Open Access Journal

Received November 29, 2018, accepted December 15, 2018, date of publication December 21, 2018,
date of current version January 11, 2019.

Digital Object Identifier 10.1109/ACCESS.2018.2888820

Carrier Aggregated Radio-Over-Fiber Downlink for Achieving 2Gbps for 5G Applications

MAHMOOD NOWEIR[1], (Student Member, IEEE), MOHAMED HELAOUI[1], (Member, IEEE), WOLFGANG TITTEL[2], and FADHEL M. GHANNOUCHI[1], (Fellow, IEEE)

[1]Radio Lab, Electrical and Computer Engineering Department, Schulich School of Engineering, University of Calgary, Calgary, AB T2N 1N4, Canada
[2]Department of Physics and Astronomy, University of Calgary, Calgary, AB T2N 1N4, Canada

Corresponding author: Mahmood Noweir (mahmood.noweir@ucalgary.ca)

This work was supported in part by Alberta Innovates Technology Futures, in part by the National Science and Engineering Research Council, and in part by the Canada Research Chair.

ABSTRACT We demonstrate experimentally, for the first time, a distributed digital predistortion model for radio-over-fiber (RoF) downlink suitable for broadband 5G signals. The model reduces the analog-to-digital converter sampling frequency up to 1/3 of the required sampling in the example of the conventional memory polynomial DPD model, hence reducing demodulator costs and hardware complexity. This model also provides better intercarrier interference by reducing the adjacent channel leakage ratio (ACLR). This leads to reduced crosstalk, which impacts the multi-core and multimode RoF links. Long-term evolution advanced signals of a 256-quadratic-amplitude modulation of different bandwidths are used to validate the model. We achieved an average reduction of 2.5 dB in ACLR for signal bandwidths in the range 100–300 MHz while maintaining minimum error vector magnitude (EVM). The RoF downlink can deliver a peak bit rate of 2.016 Gb/s with a spectral efficiency of 6.72 b/Hz and EVM less than 4%.

INDEX TERMS 5G wireless communication networks, analog to digital converter speed, digital predistortion linearization, inter carrier interference, memory polynomial, MIMO crosstalk, radio-over-fiber downlinks.

I. INTRODUCTION

The radio-over-fiber (RoF) is the enabling technology for the upcoming 5G cellular networks. This is because of its ability to carry broadband signals and provide high-speed connections and low latency [1]. It also brings advantages such as saving hardware costs, smaller footprint, less power loss, sharing resources and centralization. In principle, RoF is the technology of modulating laser light, using radio frequency (RF) signals which then propagate into a low distortion and low loss fiber optics medium. Therefore, RoF is a preferred technology to reduced capital expenditure and operational expenditure compared to traditional electronic networks.

The Mach-Zehnder modulators (MZMs) work as an electro-optic (EO) modulator, generates undesired frequency components (nonlinearity) due to its nonlinear transfer function [2]. 5G signals such as LTE-A and filter bank multi-carrier (FBMC) have high peak-to-average power ratio (PAPR) which degrades the MZM linearity even further [3]. Digital predistortion (DPD) is a well-known digital technique that is used in both optical [2]–[4], and electrical [5]–[8] transmitters to compensate for nonlinear distortion. It is obtained merely by adding a digital nonlinear block in baseband domain, which generates an inverse of the distortion of the nonlinear system.

One of the limitations of the DPD is the required observation bandwidth (BW) – the minimum BW needed at the input of analog to digital converter (ADC) in the feedback path to build the DPD – must be at least 5 times the input signal baseband BW [9]. This observation BW allows to capture the 5th order intermodulation products, hence building an approximately accurate model. To alleviate these requirements and reduce the hardware costs, Hammi *et al.* [10] proposed a distributed DPD (D-DPD) model for RF power amplifier (PA) to extend the limitation of the baseband BW. In order to test the efficacy of their technique, they varied the observation BW by changing the ADC sampling frequency f_s^{ADC} from 5 times to 2.05 times the input signal instantaneous BW. Then, they monitored the impact of the model on the spectra of the linearized signals accordingly. At low f_s^{ADC}, the D-DPD model showed a considerable improvement in the adjacent channel leakage or power ratio (ACLR or ACPR)

when compared to the conventional memory polynomial DPD (MP-DPD) model.

The bandwidth of the new radio (NR) networks, based on carrier aggregation, is going to reach 400 MHz [1] in 2020. Therefore, to build DPD models by the traditional techniques, the sampling frequency of the ADCs must be at least 2000 MHz. Such high speed ADCs are expensive and difficult to find off-the-shelf due to their fabrication complexity. The multi-core fiber is one of the multi-input multi-output (MIMO) techniques implemented in RoF links [11], [12] to increase the channel capacity and spectral efficiency. However, it is an essential requirement in multi-core and multimode fiber links [13], [14] to maintain low ACLR in order to prevent inter carrier interference (ICI) and crosstalk distortion between channels. He *et al.* [12] and Mo *et al.* [15] crosstalk cancellation algorithms for specific modulation formats with relatively complicated processing steps. Another ACLR reduction technique in RoF links was proposed in [16] by designing two successive stages, one for crest factor reduction, and the other to perform the DPD. They demonstrated a 5 dB ACLR improvement and an achieved error vector magnitude (EVM) of 7.26% for a 20 MHz LTE signal.

In this paper, to alleviate the above limitations, we implemented for the first time the D-DPD modeling technique in RoF links suitable for 5G applications. The D-DPD model reduced the needed observation BW to 500 MHz for signals with 300 MHz baseband BW, corresponds to a reduction of 1/3 as compared to conventional MP-DPD. The model will lead to reducing the ICI in multi-core and multimode fibers and provides less processing complexity and hardware costs. The experiment is performed using 6 different wideband LTE-A signals transmitted over an externally modulated RoF downlink. Spectral efficiency of 6.72 b/Hz for the 256-QAM signal is achieved as compared to 5.04 b/Hz of the 64-QAM [17].

II. THEORY AND PRINCIPLE OF OPERATION OF D-DPD IN RoF LINKS

A. CONVENTIONAL DPD MODELING

In most RoF links that are based on external modulation, the main source of nonlinearity is from the MZM transfer function [18], considering the other components in the link are set to operate in their linear regime.

The operation of the MP-DPD model shown in Fig.1 was explained in more details in [3]. In the first iteration, the predistorter blocks shown in Fig.1 are removed. The baseband discrete input signal $x[n]$, where n is the sample index, is converted to continuous analog signal by the digital to analog converter (DAC) and up converted to the frequency f_c at the up-conversion stage (UCS). Then it is transmitted through the RoF link. Due to the link nonlinearity, unwanted frequency components are generated around f_c which is visualized as spectral regrowth. To generate the DPD model, the output analog signal y_{out_RoF} is captured, frequency down-converted at the down conversion stage (DCS), and digitized to $y[n]$

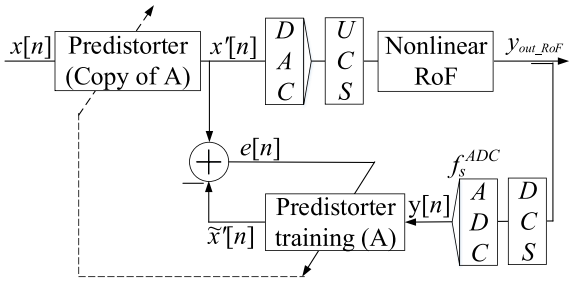

FIGURE 1. The conventional block diagram for DPD system, the ADC speed must be 5 times the baseband BW for accurate modeling.

using the ADC stage as shown in the figure. From the information of both $x[n]$ and $y[n]$, offline steps are carried out to calculate the behavior of the system and to generate the inverse DPD model [19]. This model is then applied to $x[n]$ resulting in the predistorted input signal $x'[n]$.

In the second iteration, the predistorter blocks are inserted to represent the predistortion stage in the system. The predistorted signal $x'[n]$ is then transmitted through the RoF system which works to cancel out the overall link nonlinearity. To improve the model quality, these steps are iterated until the error signal $e[n] = x'[n] - \tilde{x}'[n]$ approaches zero [2], [5]. The observation BW to build the model is controlled by the specifications of the equipment, namely the ADC sampling rate f_s^{ADC}. The higher the ADC sampling rate the wider the signal that can be linearized.

B. D-DPD MODELING

The structure of the D-DPD model is shown in the block diagram of Fig.2. The output signal $w'[n]$ from the dynamic model (in this work a MP function is used [19]) is given as:

$$w'[n] = \sum_{m=0}^{M} \sum_{k=1}^{K} h_{m,k} w[n-m]|w[n-m]|^{k-1} \tag{1}$$

where M is the memory depth, K is the nonlinear order, and $h_{m,k}$ are the coefficients of the model.

The wideband output predistorted signal $z'[n]$ from the static nonlinear predistorter shown in Fig.2 is given in [10] as:

$$z'[n] = \sum_{l=0}^{L} b_l w'[n]|w'[n]|^l \tag{2}$$

where L is the nonlinear order and b_l refers to the coefficients of the static DPD model.

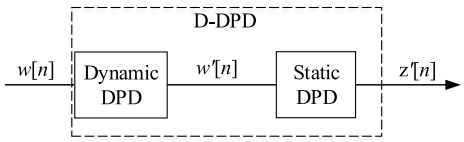

FIGURE 2. Distributed DPD model made of two stages, dynamic and statics models.

Using two cascaded DPD models resulted in distributing the overall nonlinearity order of the RoF into two lower order nonlinear functions. The D-DPD technique reduced the nonlinearity order K of the first stage MP-DPD from 10, in the case of the conventional MP-DPD model, to 3.

The steps involved in constructing a D-DPD model are summarized as:

1) Generate the static look-up table model from transmitting and capturing a narrowband 10 MHz LTE-A signal.
2) Predistort the wideband signal $w[n]$ using the previous obtained model in step 1 to get $w'[n]$.
3) Transmit the predistorted wideband signal $w'[n]$ through the RoF system and capture the output $z[n]$. Until now $z[n]$ was only compensated for static nonlinearity.
4) By processing the original input signal $w[n]$ and the static compensated output signal $z[n]$, a MP model can be generated.
5) This MP model is placed in front of the static to form the complete D-DPD block as shown in Fig.3(d).

C. CONVENTIONAL MP-DPD VERSUS D-DPD MODELING

Fig.3 illustrates the advantages of using the D-DPD model in contrast to the conventional MP-DPD model. In Fig.3(a) a narrowband signal $x[n]$ is transmitted through the RoF downlink and captured with observed spectral regrowth due to the MZM nonlinearity. A conventional 1-box DPD can adequately linearize this signal as long as the observation BW is at least five times the baseband BW of the signal, as shown in Fig.3(b). However, when the DPD observation BW is less than five times of wider BW signals, as $w[n]$ in Fig.3(c), the MP-DPD model failed to suppress the spectral regrowth completely. This shortage in the observation BW led to ACLR degradation to the output wideband signal $z[n]$.

The D-DPD, in the other hand, can completely linearize broader signals and effectively improve the ACLR as shown in the output spectrum of Fig.3(d). The D-DPD model consists of two consecutive DPD stages: the static look-up table model, and the memory polynomial model [19]. Firstly, the static model is generated by transmitting and capturing a 10 MHz narrowband LTE-A signal through the same link.

Secondly, the dynamic model is then built by dealing with the previous generated static model as part of the overall nonlinear RoF system.

D. MODEL VALIDATION METRICS

To test and compare which model performs better in reducing the out-of-band spectrum, we calculated the ACLR of the output signals. The ACLR is given as the ratio of the filtered average power of a reference channel centered at a certain carrier frequency to the filtered average power of a channel centered at adjacent frequency [20].

The EVM [20] is also used to quantify the amount of nonlinearity before and after applying the predistortion model

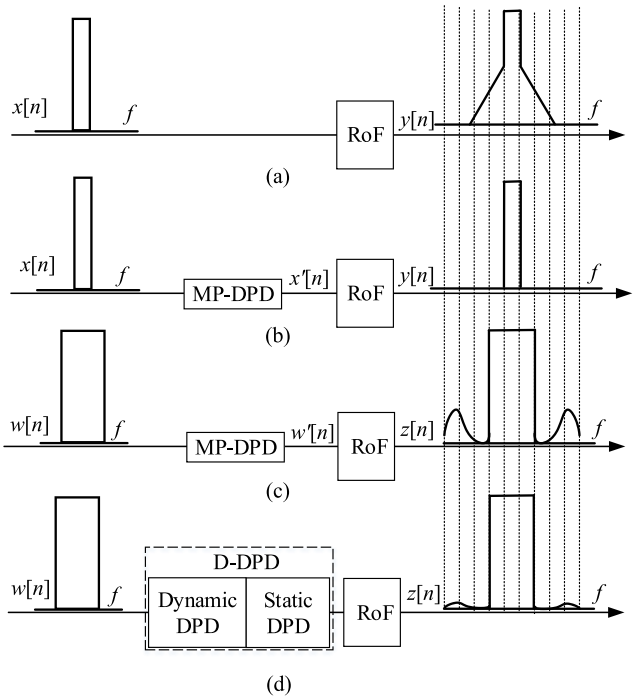

FIGURE 3. Comparison between MP-DPD and D-DPD model. (a) A narrowband signal $x[n]$ caused spectral regrowth in the output signal spectrum $y[n]$ due to the RoF link nonlinearity. (b) Conventional MP-DPD model can compensate for static and dynamic nonlinearity when the observation BW is enough. (c) Failure to properly linearize a wideband signal $w[n]$ due to shortage in the observation BW. (d) D-DPD model successfully linearized the wideband signal and improved the ACLR.

and calculated as:

$$EVM_{rms}(\%) = \sqrt{\frac{\frac{1}{N}\sum_{n=1}^{N}|y[n]-x[n]|^2}{\frac{1}{N}\sum_{n=1}^{N}|x[n]|^2}} \times 100 \qquad (3)$$

where $x[n]$ is the input baseband signal, $y[n]$ is the aligned output baseband signal, and N is the total number of time samples.

The model performance can be measured by the normalized mean square error (NMSE) [19] that is given as:

$$NMSE(dB) = 10\log_{10}\frac{\sum_{n=1}^{N}|y_{meas}[n]-y_{mod}[n]|^2}{\sum_{n=1}^{N}|y_{meas}[n]|^2} \qquad (4)$$

where $y_{meas}[n]$, $y_{mod}[n]$ are the measured and modeled output signal, respectively.

III. EXPERIMENTAL RESULTS AND DISCUSSION

As shown in Fig. 4, the experimental setup consists of a continuous wave (CW) distributed feed-back (DFB) laser lasing at a wavelength of $\lambda_o = c/f_o = 1552.93$ nm as shown in Fig.4(a) with a fixed optical power of 35 mW (c is the speed of light in vacuum). Then the MZM, which has a switching voltage of $V_\pi = 5$ V from Optilab, modulates the laser light by different LTE-A signals as shown in Fig.4(b) mixed at an RF frequency of $f_c = 4$ GHz using an Agilent-E8257D high-performance signal generator (PSG). The MZM is biased

to its quadrature transmission point (half V_π) to reduce the nonlinearity.

Six different LTE-A signals bandwidths of 256-QAM-OFDM are generated offline by MATLAB LTE toolbox and sampled by an Agilent-81180A arbitrary wave generator. The optical signal is then amplified using an Optilab erbium-doped fiber amplifier (EDFA) and propagated down through a standard single-mode telecommunication fiber of 12 km long to be directly detected by a 40 GHz photodetector (PD). The PD represents the optical-to-electrical conversion stage at the remote radio head (RRH) unit. In the end, the PD output signal is filtered at 4 GHz as shown in Fig.4(c) and analyzed by a Rohde & Schwarz FSW43 signal/spectrum analyzer (SSA).

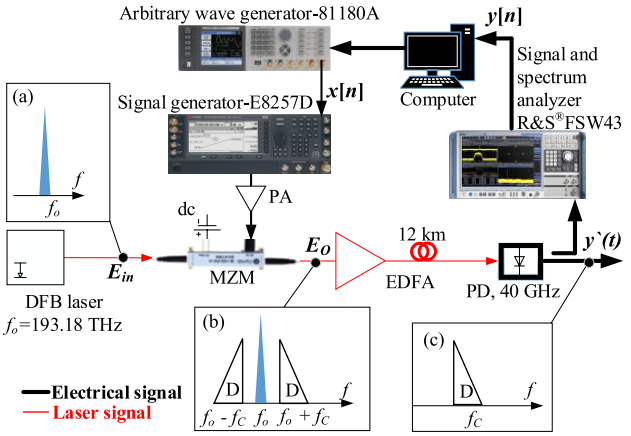

FIGURE 4. Experimental setup for the external modulation RoF downlink.

Similar to the method described in Section II, in the feedback path, the SSA is used to capture and down-convert the output signal to baseband $y[n]$. Then both the input and output signals $x[n]$ and $y[n]$ are aligned in magnitude, phase, and time offline in a computer workstation. The memory polynomial DPD model is then generated using a MATLAB code with proper order and depth.

To investigate the performance of the D-DPD model as compared to MP-DPD, a fixed sampling frequency of 500 MHz is fixed at the receiver side and six different LTE-A signals are tested independently.

As shown in Table 1, the D-DPD model improved the ACLR by an average reduction of 2.5 dB for the range of BWs from 100 MHz to 300 MHz compared to the MP-DPD.

This improvement in the ACLR values is achieved while maintaining almost the same EVM for both, the conventional MP-DPD and the D-DPD, as shown from Fig. 5. The required ADC sampling frequency is considerably reduced in the case of applying the D-DPD model as seen in Fig. 5. The achieved reduction in f_s^{ADC} from 1500 MHz to 500 MHz is equal to a reduction 1/3 the sampling frequency when applying MP-DPD model for 300 MHz BW signal.

Figures 6-11 summarize the gradual increase in the spectral side bands with increasing baseband BW in the case of the MP-DPD model. There was no noticeable change in

TABLE 1. ACLR values for no DPD, MP-DPD, and D-DPD with achieved bit rates.

Bandwidth (MHz)	ACLR (dBc)			Bit rates (Gbps)
	No DPD	MP-DPD	D-DPD	
100	-33	-47	-48	0.672
160	-32	-43	-45	1.0725
200	-32	-43	-45	1.344
240	-31	-40	-43	1.6128
280	-32	-38	-42	1.8816
300	-33	-39	-42	2.016

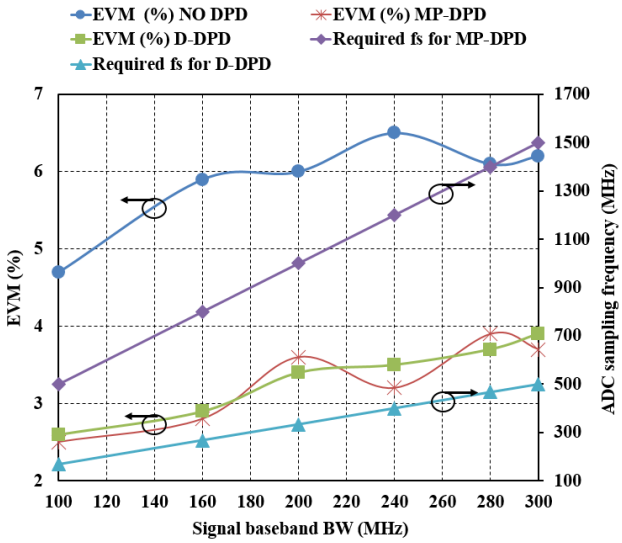

FIGURE 5. EVM without DPD and with both DPD models. And the reduction of f_s^{ADC} for D-DPD as compared to MP-DPD.

the performance between the two different models when the signal BW is 100 MHz or below, as shown in Fig. 6. The reason, as explained in Section II, is because the observation BW is large enough to construct an accurate model.

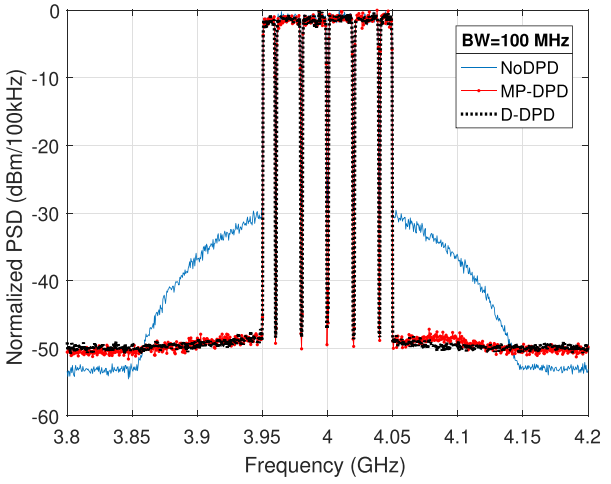

FIGURE 6. LTE-A signal spectrum at 4 GHz with sampling frequency of 500 MHz and BW of 100 MHz.

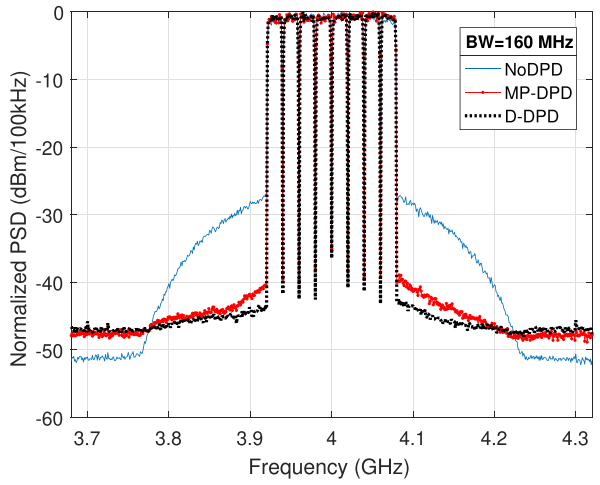

FIGURE 7. LTE-A signal spectrum at 4 GHz with sampling frequency of 500 MHz and BW of 160 MHz.

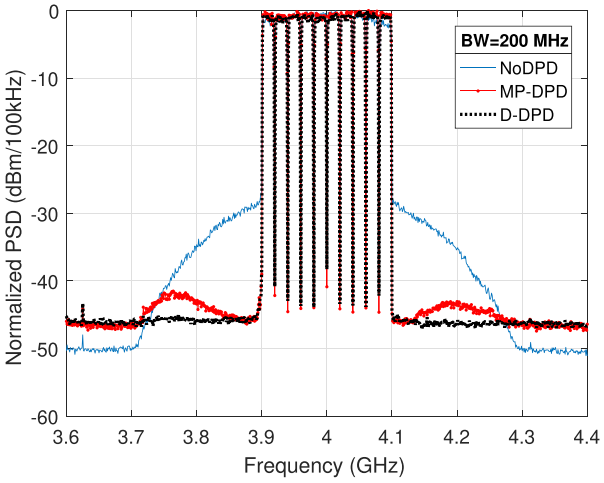

FIGURE 8. LTE-A signal spectrum at 4 GHz with sampling frequency of 500 MHz and BW of 200 MHz.

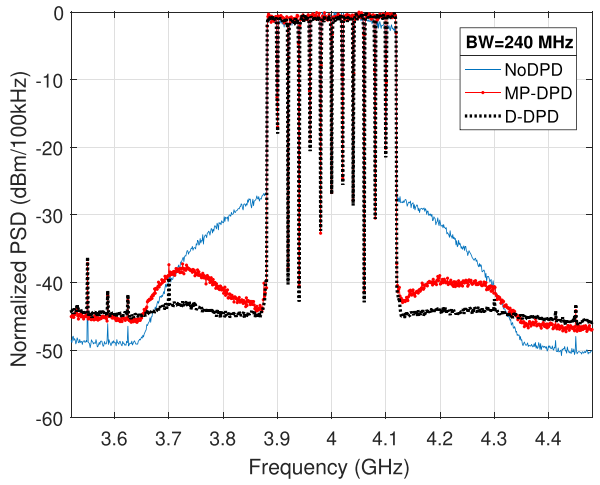

FIGURE 9. LTE-A signal spectrum at 4 GHz with sampling frequency of 500 MHz and BW of 240 MHz.

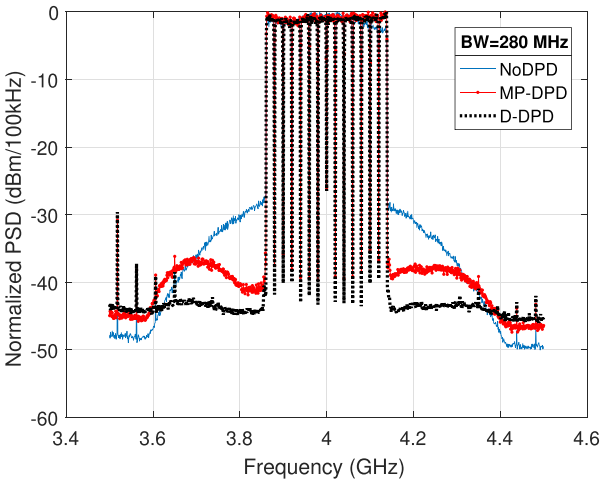

FIGURE 10. LTE-A signal spectrum at 4 GHz with sampling frequency of 500 MHz and BW of 280 MHz.

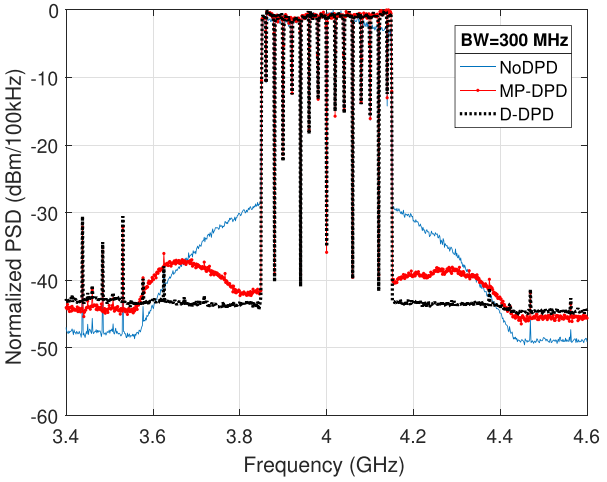

FIGURE 11. LTE-A signal spectrum at 4 GHz with sampling frequency of 500 MHz and BW of 300 MHz.

TABLE 2. List of symbols.

Symbol	Description
$e[n]$	modeling error signal
f	frequency
f_c	RF carrier frequency
f_o	Laser frequency
f_s^{ADC}	ADC sampling frequency
K	nonlinear order
M	memory depth
n	signal sample number
$w[n]$	arbitrary wideband signal
$w'[n]$	arbitrary wideband predistorted signal
$x[n]$	arbitrary narrowband input signal
$x'[n]$	arbitrary narrowband predistorted signal
$y[n]$	arbitrary narrowband output signal
$z[n]$	arbitrary wideband output signal

However, when the signal BW is increased to more than 1/5 of f_s^{ADC}, the performance of the D-DPD model in contrast to the conventional MP-DPD model is clearly observed from the spectra shown in Figs 7-11. The D-DPD model effectively suppressed the undesired spectral regrowth and improved the overall ACLR. The achieved results are important in

the multi-core and multimode fiber links where minimum leakage to the adjacent channels is needed [12].

IV. CONCLUSION

In this paper we demonstrated an effective method of reducing the ACLR for carrier aggregated LTE-A signals propagated in a single mode radio-over-fiver (RoF) downlink. The results showed useful application of the model in reducing the ICI in muti-core fiber suitable for 5G systems. The technique is performed by using a dynamic (MP-DPD) model stage for broadband signal linearization followed by a static look-up table DPD model. A reduction of the required ADC sampling frequency to 1/3 the required sampling of the conventional DPD model. An average reduction of 2.5 dB in ACLR for six LTE-A signals with baseband BWs of up to 300 MHz was achieved. By applying the model we reached to a maximum bit rate of 2.016 Gbps and a spectral efficiency of 6.72 b/Hz with an EVM less than 4 %.

ACKNOWLEDGMENTS

The authors gratefully acknowledge discussions with Dr. O. Hammi, and Mr. A. Abounemra.

REFERENCES

[1] S. Parkvall, E. Dahlman, A. Furuskar, and M. Frenne, "Nr: The new 5G radio access technology," *IEEE Commun. Standards Mag.*, vol. 1, no. 4, pp. 24–30, Dec. 2017.

[2] Y. Pei *et al.*, "Complexity-reduced digital predistortion for subcarrier multiplexed radio over fiber systems transmitting sparse multi-band RF signals," *Opt. Express*, vol. 21, no. 3, pp. 3708–3714, 2013.

[3] M. Noweir *et al.*, "Digitally linearized radio-over fiber transmitter architecture for cloud radio access network's downlink," *IEEE Trans. Microw. Theory Techn.*, vol. 66, no. 7, pp. 3564–3574, Jul. 2018.

[4] Y. Pei *et al.*, "A novel multi-channel digital pre-distortion technique for subcarrier multiplexed radio-over-fiber system," in *Proc. Opt. Fiber Commun. Conf.*, 2013, Paper. JTh2A–54.

[5] C. Eun and E. J. Powers, "A new Volterra predistorter based on the indirect learning architecture," *IEEE Trans. Signal Process.*, vol. 45, no. 1, pp. 223–227, Jan. 1997.

[6] L. Ding *et al.*, "A robust digital baseband predistorter constructed using memory polynomials," *IEEE Trans. Commun.*, vol. 52, no. 1, pp. 159–165, Jan. 2004.

[7] M. Helaoui, S. Boumaiza, A. Ghazel, and F. M. Ghannouchi, "Power and efficiency enhancement of 3G multicarrier amplifiers using digital signal processing with experimental validation," *IEEE Trans. Microw. Theory Techn.*, vol. 54, no. 4, pp. 1396–1404, Jun. 2006.

[8] J. Kim, Y. Y. Woo, J. Moon, and B. Kim, "A new wideband adaptive digital predistortion technique employing feedback linearization," *IEEE Trans. Microw. Theory Techn.*, vol. 56, no. 2, pp. 385–392, Feb. 2008.

[9] C. Yu, L. Guan, E. Zhu, and A. Zhu, "Band-limited Volterra series-based digital predistortion for wideband RF power amplifiers," *IEEE Trans. Microw. Theory Techn.*, vol. 60, no. 12, pp. 4198–4208, Dec. 2012.

[10] O. Hammi, A. Kwan, S. Bensmida, K. A. Morris, and F. M. Ghannouchi, "A digital predistortion system with extended correction bandwidth with application to LTE-A nonlinear power amplifiers," *IEEE Trans. Circuits Syst. I, Reg. Papers*, vol. 61, no. 12, pp. 3487–3495, Dec. 2014.

[11] S. Bigo, M. Salsi, O. Bertran-Pardo, J. Renaudier, and G. Charlet, "Challenges and opportunities of MIMO processing for optical transport systems," in *Proc. IET Conf.*, vol. 2, Jan. 2013, pp. 137–139.

[12] J. He *et al.*, "Experimental investigation of inter-core crosstalk tolerance of MIMO-OFDM/OQAM radio over multicore fiber system," *Opt. Express*, vol. 24, no. 12, pp. 13418–13428, 2016.

[13] B. Lee *et al.*, "120-Gb/s 100-m transmission in a single multicore multimode fiber containing six cores interfaced with a matching VCSEL array," in *Proc. IEEE Photon. Soc. Summer Topicals*, Jul. 2010, pp. 223–224.

[14] T. Huynh *et al.*, "4 × 50 Gb/s NRZ shortwave-wavelength division multiplexing VCSEL link over 50 m multimode fiber," in *Proc. Opt. Fiber Commun. Conf.*, 2017, Paper. Tu2B–5.

[15] Q. Mo *et al.*, "2 × 2 MIMO OFDM/OQAM radio signals over an elliptical core few-mode fiber," *Opt. Lett.*, vol. 41, no. 19, pp. 4546–4549, 2016.

[16] H. Chen, J. Li, C. Yin, K. Xu, Y. Dai, and F. Yin, "Multi-dimensional crest factor reduction and digital predistortion for multi-band radio-over-fiber links," *Opt. Express*, vol. 22, no. 17, pp. 20982–20993, 2014.

[17] X. Liu, H. Zeng, N. Chand, and F. Effenberger, "Efficient mobile fronthaul via DSP-based channel aggregation," *J. Lightw. Technol.*, vol. 34, no. 6, pp. 1556–1564, Mar. 15, 2016.

[18] B. Masella and X. Zhang, "Linearized optical single sideband Mach–Zehnder electro-optic modulator for radio over fiber systems," *Opt. Express*, vol. 16, no. 12, pp. 9181–9190, 2008.

[19] F. M. Ghannouchi, O. Hammi, and M. Helaoui, *Behavioral Modeling and Predistortion of Wideband Wireless Transmitters*. Hoboken, NJ, USA: Wiley, 2015.

[20] *Evolved Universal Terrestrial Radio Access (EUTRA); Base Station (BS) Conformance Testing (Release 14)*, document TS 36.141 v14.1.0, 3GPP, Sep. 2016.

MAHMOOD NOWEIR (S'17) received the B.Sc. degree in electrical engineering from the University of Tripoli, Tripoli, Libya, in 2002, and the M.Sc. degree in electrical and computer engineering from RIT, Rochester, NY, USA, in 2010. He is currently pursuing the Ph.D. degree with the University of Calgary, Calgary, AB, Canada. His current research interests include impairments mitigation of radio-over-fiber links, millimeter-wave generation, and 5G system development.

MOHAMED HELAOUI (S'06–M'09) received the M.Sc. and Ph.D. degrees in communications and information technology from the École Supérieure des Communications de Tunis, Ariana, Tunisia, in 2003 and 2006, respectively, and the Ph.D. degree in electrical engineering from the University of Calgary, Calgary, AB, Canada, in 2008. He is currently an Associate Professor with the Department of Electrical and Computer Engineering, University of Calgary. His current research interests include digital signal processing, power efficiency enhancement for wireless transmitters, efficient and broadband power amplifiers, MMIC power amplifiers for wireless and satellite communications, six-port receivers and advanced transceiver design for software-defined radio, and millimeter-wave applications. His research activities have led to more than 150 publications, one book, three book chapters, and 11 patent applications (seven of them are granted). He is also the Chair of the Southern Alberta Section, IEEE local COM/MTT/AP Joint Chapter.

WOLFGANG TITTEL is currently a Professor with the Department of Physics and Astronomy, University of Calgary, where he is also with the Institute for Quantum Science and Technology. He is engaged in ground-breaking experiments in the field of quantum communication from early stages on. The investigations were seminal in bringing the new quantum technology out of the laboratory and into the real world using a standard telecommunication fiber network, thereby raising both scientific and public awareness and appreciation that it is not restricted to the contrived laboratory settings. He has authored or co-authored nearly 100 articles in refereed journals (cited in total of more than 17 000 times). His research interests include practical quantum cryptography, quantum memory, quantum repeaters, and quantum networks. He is a Senior Fellow of the Canadian Institute for Advanced Research and an Editorial Board Member of *Quantum Science and Technology* (IOP). He is currently the AITF Strategic Research Chair of Quantum Secured Communications.

FADHEL M. GHANNOUCHI (S'84–M'88–SM'93–F'07) is currently a Professor, the Alberta Innovate Strategic Chair of Intelligent RF Technology, the Canada Research Chair of Green Radio Systems, and the Director of iRadio Lab, University of Calgary, Canada. He is also a part-time 1000 Talent Professor with the Department of Electronic Engineering, Tsinghua University, Beijing, China. His research interests include microwave, wireless, and optical communications. He is a Fellow the Institution of Engineering and Technology, The Canadian Academy of Engineering, The Engineering Institute of Canada, and the Academy of Science of the Royal Society of Canada.